JSST
Journal of Space Science & Technology

Vol. 2, No. 5, Fall 2009 and Winter 2010
pp. 1-14

Electro-Optical Design of Imaging Payload for a Remote Sensing Satellite

E. Peighani-Asl[1*], D. Abbasi-Moghadam[2], B. Ghafary[3] and V. Tabataba-Vakili[4]

1, 2, 3 and 4. Iran University of Science and Technology

*Ave. Farjam, Tehran, IRAN

ha_laser@yahoo.com

Remote sensing using small spacecraft arising from multi-objective economic activity problems is getting more and more developed. These satellites require very accurate pointing to specific locations of interest, with high reliability and small latency. The space borne imaging systems always attempted to achieve the highest ground resolution possible with the available technology at the given time. Also mass, volume and power consumption of the spacecrafts and instruments followed the trend to miniaturization. But the most promising prospects for high resolution imaging with remote sensing satellites are connected with passive optical systems, especially push broom systems. In this paper optical system design process is described and different parameters of this process such as MTF, SNR, FOV, aperture diameter, stability and pointing, scanning schemes, detector selection, and target radiance are simulated and analyzed.

Keywords: MTF, SNR, push broom, detector, imaging payload, stability

Introduction

High resolution mapping systems follow the trend to smaller Ground Sample Distances (GSD). The increasing number of space borne imaging systems in the last decade (see [1] for more) shows that an increasing number of countries are dealing with space borne technology and that there is an increasing need for mapping systems for different applications [2]. The trend to smaller GSDs was and is supported by the improvements in diverse fields of technology for instance optics, mechanics and materials, electronics, signal processing, communication and navigation. Active micro wave systems, e.g. SAR systems, are an alternative to passive optical mapping systems. They also benefit from the technology improvements. But the most promising prospects for high resolution mapping with small satellites are connected with passive optical systems, especially push-broom systems. High resolution optical systems on small satellites have to overcome a couple of problems. In this paper we consider a GSD of 10 m or less as high resolution, and a satellite with 1000 kg or less mass as a small satellite according to the IAA Study Cost-Effective Earth Observation Missions [3].

Smaller GSD needs larger focal lengths. The physics behind optical systems allows only a restricted number of tricks to overcome the problems of large focal length optics in terms of volume and mass. The size of the focal plane depends on the detector system size and is part of the equation concerning optics volume and mass. The pointing stability is said to be too low using small satellites. What are the requirements and restrictions? The large amounts of date of high resolution imaging systems need to be stored and transmitted using high performance devices. Size, mass and power consumption of those devices increases with increasing data volumes and data rates. High resolution means also to deal with small amounts of energy coming from small ground pixels to be registered in small integration time periods according to the high satellite orbit velocities. So, the question is how far can we go with decreasing the GSD (increasing the ground resolution) using small satellites?

Civil space borne Earth surface mapping started in 1972 with an 80 m GSD provided by ERTS, later renamed to Landsat-1. Nowadays, the GSD approaches 1 m or even less. The electro-optic complex is intended for a panchromatic and spectrozonal survey of Earth surface. Cameras provide reception of optical radiation from Earth surface and

1.M.Sc. of Iran University of Science and Technology (Corresponding Author)
2.PhD. Student in Iran University of Science and Technology
3. Professor in Iran University of Science and Technology
4.Associate Professor in Iran University of Science and Technology

transformation of optical image into digital electrical signal. Structure of a typical electro-optic complex, based on CCD, is presented on figure (1).

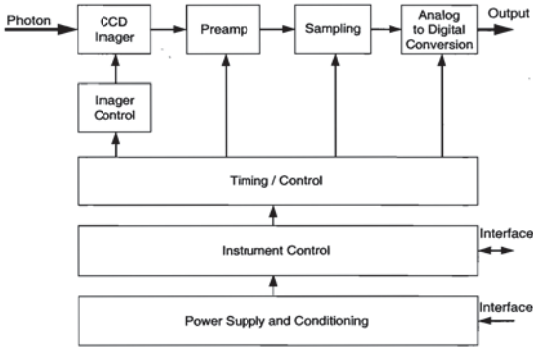

Fig. 1. Structure of electro-optical system complex

Some major features are considered which influence the image quality from the spatial resolution point of view. A very effective way to describe the image quality is to use the Modulation Transfer Function MTF. Using the MTF approach, you can multiply all the image quality influencing MTF components of a linear system (or quasi linear system) which may be based on different physical effects (e. g. optics, CCD, electronics …) in order to create the system MTF. The resulting Point Spread Function (PSF) of the system is then computed applying the Inverse Fourier Transform (IFT).

Limits of electro-optical systems designing

Diffraction

For most of the operating systems, the optical system may be considered near diffraction limited and in focus. This diffraction causes a diffraction disc or Airy disc. The Airy disc diameter d caused by diffraction is derived from PSF_{optics} [4]. It is one of the important parameters which can be related to the detector pixel size x:

$$d = 2.44.\lambda.\frac{f}{D} = 2.44.\lambda.F \qquad (1)$$

where f is the focal length, D is the aperture of the optics, and λ is the average wavelength of the radiation. If x is larger than d the system is detector limited, and the resolution is determined by the detector. Otherwise the optics determines the spatial resolution. Figure (2) shows the borderline for an average wavelength of λ=0.55 μm (green). The optics designs should be near to the borderline on the optics limited side in order to get maximum energy for the detector avoiding too large aliasing effects. For state-of-the-art CCD detectors with a pitch of 7 μm, an f/5.2 optics would satisfy this approach.

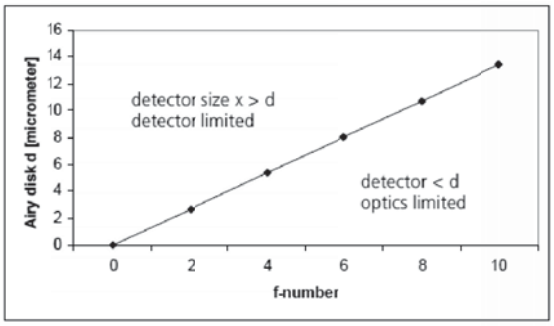

Fig. 2. Airy disk parameter d as a function of the f-number F (λ=0.55 μm) [8]

Aberrations

Aberrations are imaging failures in the image plane if the diffraction is ignored. Aberrations lead to an additional smearing effect (additional to the diffraction). It can be differentiated in monochromatic and chromatic aberrations (see table 1) [5].

Table 1. Aberrations that can be corrected by the three Basic optical systems [5]

Image Error	Double/ Schmidt	Teleoptic / Cassegrain	Triplet/ TMA
Lateral Chromatic Aberration	√	√	√
Length Chromatic Aberration	√	√	√
Spherical Aberration	√	√	√
Coma	√	√	√
Astigmatism		(√)	√
Distortion	(√)	(√)	√
Curvature of Field		(√)	√

Chromatic Aberration

Usually associated with objective lenses of refractor telescopes. It is the failure of a lens to bring light of different wavelengths (colors) to a common focus. This results mainly in a faint colored halo (usually violet) around bright stars, the planets and the moon. It also reduces lunar and planetary contrast. It usually shows up more as speed and aperture increase. Achromat doublets in refractors help reduce this aberration and more expensive, sophisticated designs like apochromats and those using fluorite lenses can virtually eliminate it.

Spherical Aberration

Causes light rays passing through a lens (or reflected from a mirror) at different distances from the optical center to come to focus at different points on the axis. This causes a star to be seen as a blurred disk rather than a sharp point. Most telescopes are designed to eliminate this aberration.

Coma
Associated mainly with parabolic reflector telescopes which affect the off-axis images and are more pronounced near the edges of the field of view. The images seen produce a V-shaped appearance. The faster the focal ratio, the more coma that will be seen near the edge although the center of the field (approximately a circle, which in mm is the square of the focal ratio) will still be coma-free in well-designed and manufactured instruments.

Astigmatism
A lens aberration that elongates images which change from a horizontal to a vertical position on opposite sides of the best focus. It is generally associated with poorly made optics or collimation errors.

Distortion
The alteration of the original shape (or other characteristic) of an object, image, sound, waveform or other form of information or representation. These distortions are minimized by using symmetric doublets.

Field Curvature
Caused by the light rays not all coming to a sharp focus in the same plane. The center of the field may be sharp and in focus but the edges are out of focus and vice versa.

Design of Electro-Optical System Parameters

Optical System Design Process consists of:

1. Determine Instrument Requirements
2. Choose preliminary aperture
3. Determine target radiance
4. Select detector candidates
5. "Optical Link Budget", SNR considerations
6. Determine Focal Plane architecture and scanning schemes
7. Select F# and telescope/optical train design
8. Complete preliminary design and check MTF
9. Determine ACS requirements

Determine Instrument Requirements
The choice of the short-wave (left) border of the panchromatic band is generally conditioned by factual peculiarities of the atmosphere.

Figure (3) shows that the Earth surface illumination when λ=0.4μm is almost 30 percent, less than when λ=0.5μm, and the atmospheric fog brightness is 10 – 15 per cent more and atmospheric fog brightness for different Sun angles above horizon. The atmospheric fog influences the quality of images received, as it reduces the general contrast of the image and the signal/noise relation. This leads to the details of low contrast at the image.

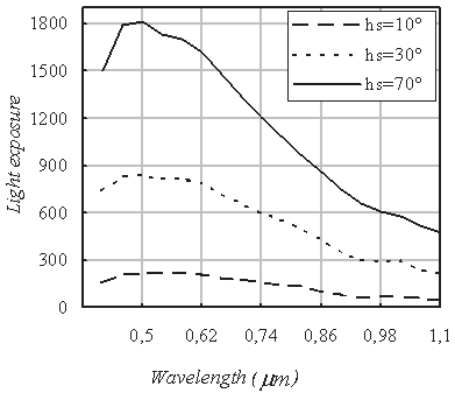

Fig. 3. Light exposure of a terrestrial surface (E), W/m^2

Another important reason for the choice of the short-wave border of the panchromatic band ≥0.5 μm is difficulty in the objective achromatization in the spectral band from 0.4 to 0.5 μm because it requires usage of the special ultraviolet glass which makes optical system much more complicated.

The choice of the long-wave (right) border of the panchromatic band rides on the physical peculiarities of the CCD causing the deterioration of the modulation transmission function in the long-wave band due to generating of the carrier inside of silicon.

The deterioration of the MTF of the multiple-unit linear photo transmitter is caused by the fact that the depth of photon absorption depends on longer waves. Figure (4) shows how the absorption factor depends on wave length and the energy of the photons of pure silicon. The α absorption factor is a possibility of photon absorption per unit of length of the way made by light inside the substance. Thus the depth of photon absorption has inverse relationship with the absorption factor. If photons are absorbed outside of the depleted area, the probability of gathering the generated charge by the appropriate sensitive element falls as far as charge moves by diffusion. This leads to the total MTF deterioration.

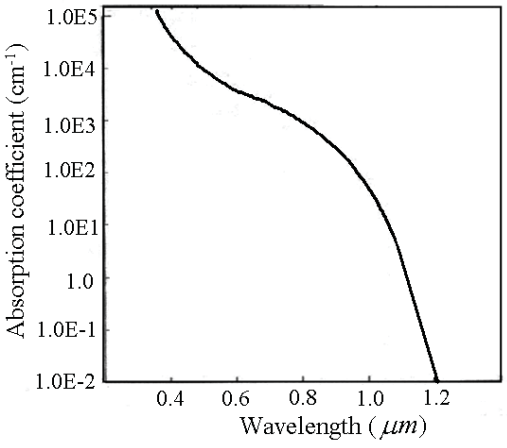

Fig. 4. Photon absorption in CCD

Determine aperture diameter

The aperture is the hole in a camera that allows light to hit film. The amount of light that gets through the aperture determines what a picture will look like. The larger the aperture, the more light it collects and the brighter (and better) the image will be. Greater detail and image clarity will be apparent as aperture increases. Aperture diameter determined by:

$$D = 2.44\,\lambda \frac{f}{d} Q \qquad (2)$$

where Q is quality factor. Quality factor is ratio of pixel size d to diameter of diffraction disk D_{Airy}, defined $Q = d / D_{Airy}$. Q typically varied between 0.5 and 2. For Q<1, the resolution is limited by diffraction in the optics and for Q>1, the resolution is limited by pixel size. As a starting point for the design, select Q=1(see figure 5) [4].

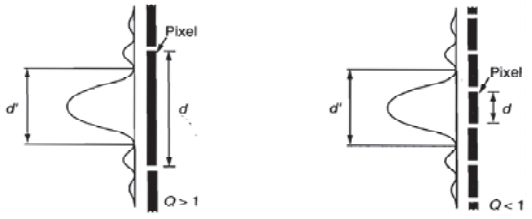

Fig. 5. Effect of Varying Quality Factor [9]

Determine target radiance

The total amount of received spectral radiance of the target at the orbit altitude (H) obtains by this equation:

$$L_{tot}(\lambda) = \frac{\rho_\lambda . \tau(\lambda) . E_\lambda}{\pi} + L_p \qquad (3)$$

where E_λ is the solar/lunar spectral radiance at orbit altitude (H) from the earth surface or target, $\tau(\lambda)$ is called atmospheric transmittance in the path (target to sensor), ρ_λ is spectral reflection coefficient of target (see figure 6), and L_p is the sum of the multiple scattered solar and atmospheric emitted radiance into the path. Figure (7) shows target radiance intensity with ρ=0.9 [6].

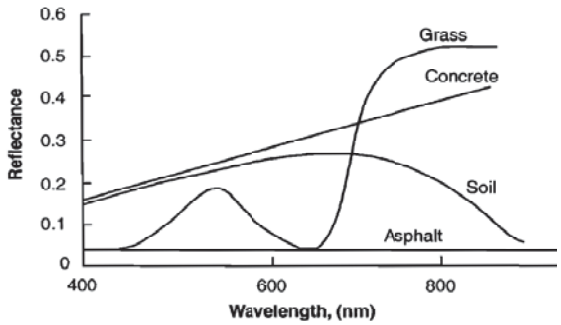

Fig. 6. Typical spectral reflectance curves for grass, concrete, soil, and asphalt [12]

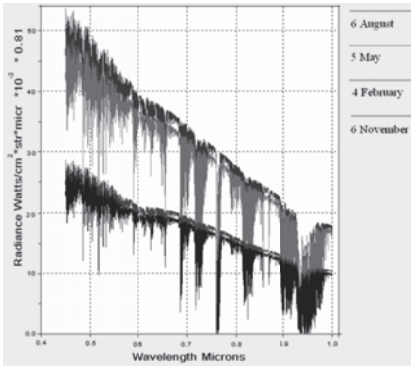

Fig. 7. Target radiance intensity in deferent wavelengths

Detectors

The easiest for realizing is scanning of the systems based on the multielement linear photodetector, for example linear CCD, photographic plate. In this case equipment via an axle is directed to the Earth, usually to the nadir. The linear field (linear photodetector) of the camera is situated obliquely to the flight direction. Scanning (storage) and electrical signals reading is performed in series from all the elements of the photodetector line and then a new period of the signal storage and reading begins (see table 2) [7].

Table 2. Detectors type characteristics [7]

Type	Sensitivity (QE)	Remarks
Film	~0.01	Non-linear • Dyn. Range: 1/100 • Detector is memory • High capacity
Photo Multiplier Tube	0.1 ... 0.3	• Photocathode, SE – Multiplier (106 ... 107) • distortions
Micro Channel Plate	0.1 ... 0.2	• Photocathode, SE - Multiplier (106 ... 107) • no distortions
CCD	0.3 ... 0.9	• Dyn. Range to 1/1000,Limited by photon noise • Very sensitive • Linear system (200000 e-/ pixel) • High capacity

Optical link budget (Signal to Noise Ratio (SNR))

One more important parameter of the electro-optic camera for the remote sensing is the relation of the signal at the zero spatial frequency $\psi 0$, that can be expressed from the given lens aperture. It is evident that each of the spectral channels may have its own relation signal/noise $\psi 0_i$ [8].

$$\psi_{0i} = \frac{1}{4} \cdot \left(\frac{D}{f}\right)^2 \cdot \frac{d^2 \cdot T_{\text{int}}}{hc \cdot N_0} \cdot \left\{ \int_{\lambda_1}^{\lambda_2} E_S(\lambda).\rho(\lambda) \times \tau_{ob}(\lambda).\tau_f(\lambda).\tau_{atm}(\lambda).\eta(\lambda)\,\lambda\, d\lambda \right\} \qquad (4)$$

where $\psi 0_i$is the signal to noise ratio at the zero spatial frequency, D is the objective diameter, f is the

objective focal distance, h is Planck's constant, c is the velocity of light, d is the element dimensions (d × d), $E_S(\lambda)$ is the earth surface illumination by the Sun, $\tau_{ob}(\lambda)$ is the objective transmission, $\tau_f(\lambda)$ is the Light filter transmission through the spectral channel λ1 - λ2, $\tau_{atm}(\lambda)$ is the atmosphere transmission, $\rho(\lambda)$ is the Earth surface reflectance, T_{int} is the storage time of the photosensitive CCD, $\eta(\lambda)$ is the effective quantum efficiency of the photosensitive CCD and N_0 is signal value (electrons), corresponding to one of quantization levels of the analog-digital converter(see figures 8 & 9).

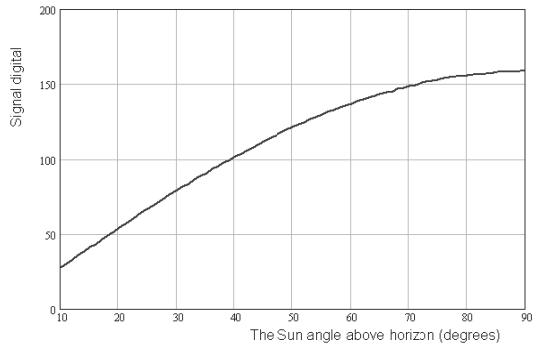

Fig. 8. Signal intensity in deferent sun angles

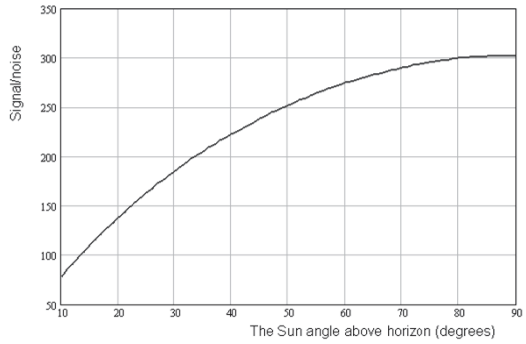

Fig. 9. Signal to noise ratio in deferent sun angles

The calculation results show that panchromatic camera provides high signal volume within all the observation conditions. When there is a high reflectance (clouds, desert), it is necessary to use the mode with reduced storage time, for example 0.5 of nominal. When the reflectance is normal, survey should be provide within a nominal storage time.

Once the detector is selected, d and $\eta(\lambda)$ are given. $E_S(\lambda)$ is also given as well as F(f/D) and $\tau_{ob}(\lambda)$ when the optics is selected or designed taking into account the technological and/or the mission constraints. $\Delta\lambda$ is fixed in most cases, so that the only real variable part is the integration time tint. For a satellite in LEO, the satellite ground track velocity is about 7 km/s. In other words, the dwell time is 1 ms for a ground sample distance GSD of 7 m. For high resolution imagers with GSD of about 1 m, tint < 1/7 ms is too short for a sufficient good signal and SNR.

$$t_{dwell}(1m)/t_{dwell}(10m) = 1/10 \tag{5}$$

Even more severe is the influence of the pixel field of view (IFOV).

$$IFOV(1m)/IFOV(10m) = 1/100 \tag{6}$$

Taking both aspects into account, reducing the GSD by a factor of 10^{-1} causes a time related and geometry related decrease of energy at the detector of about 10^{-3}.

There are two possibilities to overcome this obstacle:

- Use TDI (Time Delay and Integration) technology with N stages in order to increase the signal N-fold and improve the SNR by the factor of $\sqrt{N}$ (this technique is used e. g. in the IKONOS and Quick Bird missions)
- Use the so-called slow-down mode in order to decrease the ground track velocity of the line projection on the surface (those technique is used for instance in the EROS-A1 mission) with respect to the satellite velocity in order to obtain the necessary dwell time t_{dwell}.

Noise components are:

Total noise equivalent irradiance is expressed in

$$< n_{tot}^2 >=< n_{ph}^2 > + < n_{dar}^2 > + < n_{sys}^2 > \tag{7}$$

Photon noise: signal + optics + field-stop + cold-shield + background

$$< n_{ph}^2 >=< n_s^2 > + < n_{op}^2 > + < n_{fs}^2 > + < n_{cs}^2 > + < n_{bg}^2 > \tag{8}$$

Electronic noise: detector + amplifier + readout + digitization

$$< n_{dar}^2 >=< n_{\det}^2 > + < n_{amp}^2 > + < n_{ro}^2 > + < n_{dig}^2 > \tag{9}$$

Systematic: cross-talk + . . . etc:

$$< n_{sys}^2 >=< n_{xt}^2 > + \cdots \tag{10}$$

All of the above noise equivalent irradiances are referenced at the detector. The selection of the surface of the detector as the SNR reference point needs some elaboration. When evaluating the system SNR, the Signal and system noise σ_{system} can be referenced at any point in the system - at the aperture, between the optical train and filter, at the detector, at the amplifier etc. This paper references the surface of the detector because it is an electro-optical system's natural optical electronic interface [8].

Where the optics, field-stop, and cold shield are modeled as thermal sources, while signal and background radiances tend to cover the entire spectrum.

Note that a good design requires proper matching of system and cold-shield solid angle. Hence, requires w_{cs} ,w_{sys}, with

$$w_{sys} = \frac{\pi}{4(f_l / D_\circ)} [sr] \tag{11}$$

Expressions evaluating the noise equivalent irradiance for signal, background, optical train, field-stop, and cold shield follow.

Signal:

$$< n_s >= \sqrt{\frac{k_d \Delta f}{A_d \eta_d} \Phi_s} = \sqrt{\frac{k_d \Delta f w_s}{A_d \eta_d hc} \int_{\lambda_{\eta 1}}^{\lambda_{\eta 2}} L_s(\lambda) \chi(\lambda) \lambda d\lambda} \quad [ph/m^2 - s] \tag{12}$$

Where $x(\lambda)$ is the system transmission, Δf is the noise equivalent bandwidth in Hertz of the band, and is normally given by $\Delta f = (2\tau_\circ)^{-1}$, $\tau_\circ =$ effective integration time (single sample or multiple time delay and integrate samples may be used), A_d the detector area, and k_d the noise process scale factor ($k_d = 2$ for a photovoltaic and $k_d = 4$ for photoconductor).

Background:

$$< n_{bg} >= \sqrt{\frac{k_d \Delta f w_\circ}{A_d \eta_d hc} \int_{\lambda_{\eta 1}}^{\lambda_{\eta 2}} L_{bg}(\lambda) \chi(\lambda) \lambda d\lambda} \quad [ph/m^2 - s] \tag{13}$$

Optical train:

$$< n_{op} >= \sqrt{\frac{k_d \Delta f w_{sys}}{\pi\ A_d \eta_d hc} \int_{\lambda_{\eta 1}}^{\lambda_{\eta 2}} \sum_i M_{op}(T_{opi}, \varepsilon_{opi}, \lambda) \frac{x(\lambda)}{T_{o_i}} \lambda d\lambda} \quad [ph/m^2 - s] \tag{14}$$

Where each optical element or optical subsystem, i=1,2,3,…,n contributes to the near-field thermal exitance M_{op}. Note how the remaining optical transmission from the ith component to the detector surface is maintained by dividing the system transmission $x(\lambda)$ by the ith component of T_0. In many cases, especially when designing a new system, a priori knowledge of the number, position, temperature, and material properties of the optical elements is unavailable. However, an $< n_{op} >$ budget can be allocated by approximating the thermal exitance with a single source,

$$< n_{op} >= \sqrt{\frac{k_d \Delta f\ \Omega_{sys}}{\pi\ A_d \eta_d hc} \int_{\lambda_{\eta 1}}^{\lambda_{\eta 2}} M_{op}(T_{op}, \varepsilon_{op}, \lambda) \frac{x(\lambda)}{T_o} \lambda d\lambda} \quad [ph/m^2 - s] \tag{15}$$

Typically, an $\varepsilon_{op} \approx 0.05 - 0.1 @ T_{op} = 300K$ will suffice for uncooled optics, where ε_{op} is the effective emissivity, and $T_{op}[^\circ K]$ is the effective temperature.

Field stop:

$$< n_{fs} >= \begin{cases} 0 & if \quad w_{cs} < w_{sys} \quad else \\ \sqrt{\frac{k_d \Delta f\ (w_{cs} - w_{sys})}{\pi\ A_d\ \eta_d hc} \int_{\lambda_{\eta 1}}^{\lambda_{\eta 2}} M_{fs}(T_{fs}, \varepsilon_{fs}, \lambda) \frac{x(\lambda)}{T_o} \lambda d\lambda} \\ [ph/m^2 - s] \end{cases} \tag{16}$$

Cold-shield:

$$< n_{cs} >= \sqrt{\frac{k_d \Delta f\ (\pi - w_{cs})}{\pi\ A_d\ \eta_d hc} \int_{\lambda_{\eta 1}}^{\lambda_{\eta 2}} M_{cs}(T_{css}, \varepsilon_{css}, \lambda) \frac{x(\lambda)}{T_o} \lambda d\lambda} \quad [ph/m^2 - s] \tag{17}$$

The exitance functions, M_{op}, M_{fs} and M_{cs} are of the form

$$M(T, \varepsilon, \lambda) d\lambda = \frac{2\pi hc^2}{\lambda^2} \varepsilon\ e^{\frac{hc}{\lambda k_b T}} d\lambda \qquad [W/m^2] \tag{18}$$

where $k_b = 1.381 \times 10^{-23}\ [J/K]$ is Boltzmann constant, ε is emissivity, and $T[^\circ K]$ is the temperature. Signal and background radiances, $L_S(\lambda) d\lambda$ and $L_{bg}(\lambda) d\lambda$ $[w/m^2 - sr]$, from a given scene that include complex transmission, backscatter, and emission effects can be generated with computer simulation tools such as LOWTRAN or MODTRAN by PCModWin 4.0 software.

When the ADC is matched to the amplifier output then

$$< n_{dig} >= \frac{N_{WELL}}{2^N \sqrt{12}} \tag{19}$$

where N_{WEEL} is the charge well capacity and N number of bits. Ideally, $< n_{dig} >$ is less than the noise floor. This is achieved by selecting a high resolution ADC (large N).

The remaining two noise terms, electronic $< n_{dar} >$ and systematic $< n_{sys} >$ will not be pursued any further except within the context of establishing a synthesis-requirement noise budget based on top-level Sensitivity performance requirements (SNR analysis). Once an $< n_{dar} >$ budget is defined, a technology-dependent feasibility study is performed to identify a candidate technology that meets the $< n_{dar} >$ budget. If no appropriate candidate is found to fulfill the synthesis requirements, the system design is iterated until an acceptable compromise between performance and synthesis is achieved. As a final observation, note that band leakage is a form of systematic noise through spectral cross-talk. Note that correlated noise ($1/f$, drift etc.) and white noise are not separated in the $< n >$ terms. When large enough, this type of correlated noise must be reduced by system calibration

in order to avoid imaging artifacts and/or radiometric errors.

In most common remote sensing sensors, namely cameras, the SNR will be in the order of 55 dB, or a ratio of 562: 1. That is, the signal is 562 times greater than the noise signal. At this ratio the noise will be unnoticeable. The following guidelines interpret some ratios of signal-to-noise in terms of the subjective picture quality.

Determine Focal Plane architecture and Scanning Schemes

There are three different scanning systems for acquiring the image (figure 10) [9]:

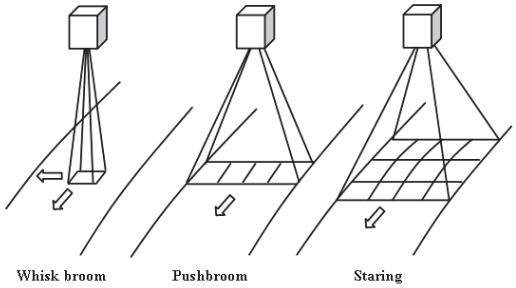

Fig. 10. Image Acquisition Modes [9]

(1) Whiskbroom imagers are working as electromechanical scanners. On-axis optics or telescopes with scan mirrors sweep from one edge of the swath to the other. The FOV of the scanner can be detected by a single detector or a single-line-detector. Simultaneously the movement of the satellite guarantees the sweeping scan over the earth. This means that the dwell time for each ground cell must be very short at a given IFOV because each scanned line consists of multiple ground cells, which will be detected. A well-known example of whiskbroom imager is AVHRR, Landsat and SeaWiFS.

(2) Push broom scanners: As electronically scanners they use a line of detectors to scan over a two dimensional scene. The number of pixels is equal to the number of ground cells for a given swath. The motion of the satellite provides the scan in along-track-direction, thus, the inverse of the line frequency is equal to the pixel dwell time. By using a two dimensional detector, one dimension can represent the swath width (spatial dimension, y) and the other the spectral range. These imaging spectrometers can be subdivided in Wide Field Imagers (MERIS, ROSIS) and Narrow Field Imagers (HSI, PRISM). By regarding space borne systems these imager-types conduce to high or frequent global coverage.

(3) Staring imagers: these imagers are also electronically scanners. They detect a two dimensional FOV at once. The IFOV along and cross track corresponds to the two dimensions of detector area array. Two subgroups of staring imagers are Wedge Imaging Spectrometer (WIS) and Time Delay Integration Imagers (TDI). If the incoming light passes a linear wedge filter each row X_n of the ground segment is seized by the detector row X_n for a determined wavelength. For very high ground resolution and low sensitivity applications, X_n rows of the ground can be traced by using a TDI. The light from the scene will be separated by a linear filter for spectral band definition. On the 2D-detector the signal for this line can be read out from multiple rows caused by the forward movement of the sensor. Therefore the sensitivity of a TDI with n rows is n times that of an imager using the push broom principle.

Push broom scanner is selected because these schemes have flowed advantages (see tables 3&4):

- large Swath width and high resolution feasible (depending on pixel number)
- relatively “long” dwell time for each pixel
- high geometric accuracy across the flight direction
- No movable parts

Table 3. Comparison of optical sensor scanning methods [9]

Scanning technique	Advantages	Disadvantages
Whiskbroom scanner-single detector element	-High uniformity of the response function over the scene - Relatively simple optics	-short dwell time per pixel -high bandwidth requirement and time response of the detector
Whiskbroom scanner-multiple detector elements	-Uniformity of the response function over the swath - Relatively simple optics	-Relatively high bandwidth and time response of the detector
Pushbroom Sensor	-Uniform response function in the along-track direction - Relatively long dwell time	-High number of pixels per line imager required -Relatively complex optics
Step-and-Stare Imager with Detector Matrix	-well defined geometry within the image - long integration time (if motion compensation is performed)	-High number of pixels per matrix imager required -complex optics required to cover the full image size -Calibration of fixed pattern noise for each pixel -Highly complex scanner required if motion compensation is performed.

Table 4. Characteristics of imagers [12]

Characteristic	LINE imager	Matrix Imager
Pixels	6000-9000	Up to 1024×1024 image pixels in frame transfer mode
Photo response nonuniformity	5%	5%
Dark signal nonuniformity	5%	5%
Dynamic range	10000	5000

Select F# and Telescope/Optical Train Design

Electro - optical system types

A telescope is an instrument designed for the observation of remote objects. The term usually refers to optical telescopes, but there are telescopes for most of the spectrum of electromagnetic radiation and for other signal types. For example, optical telescope, radio telescopes, X-ray and gamma-ray telescopes [9].

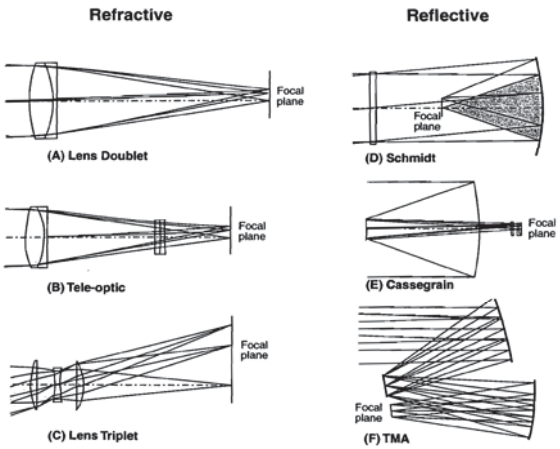

Fig. 11. Basic configurations for Refractive and Reflective optical systems [5]

Electro-optical systems divided into two classifications: reflective systems using specular reflection and refractive systems using optical lens systems (see figure 11). Reflective system is selected because these schemes have flowed advantages:

1. Only one surface of an optical element has to be manufactured with high precision (the mirror)
2. The backside can be lightweight
3. High numerical aperture feasible
4. distortions and optical performance are not dependent from the wavelength
5. Many different materials are suitable for a mirror (optical glasses, metals, Zerodur, SiC, etc.)

Infinity F-number or F-stop is defined as:

$$F\# = f/D \tag{20}$$

where D is the aperture or diameter of the system.

F-number indicates the amount that the lens can open up or close down to let in more or less light, respectively. The greater the F-number, the less light per unit area reaches the image plane of the system.

Consequently image brightness is proportional to:

$$I \propto 1/F\#^2 = D^2/f^2 \tag{21}$$

In table 5 electro-optical system types advantages and drawbacks are shown.

Table 5. Electro-optical system types advantages and drawbacks [9]

Optics	Advantages	Drawbacks
Refractive	•Low costs because of spherical lens surfaces •High image quality and strong light signal possible, because of no obscuration by mechanical elements •Inexpensive optic adjustment by circular lenses and axial locations •Diversity of optical lens materials allows spectral corrections in a wide range of applications •Stray light suppression by simple baffle arrangements possible	•No long focal length with high aperture numbers possible •Chromatic aberrations at high spectral band with (> 200nm) have to be corrected
Reflective	•Only one surface of an optical element has to be manufactured with high precision (the mrror) •The backside can be lightweight •High numerical aperture feasible •distortions and optical performance are not dependent from the wavelength •Many different materials are suitable for a mirror (optical glasses, metals, Zerodur, SiC, etc.)	•For small Field of Views only •More expensive in manufacturing, assembly and integration (higher precision) •Obscuration due to supporting elements for secondary mirror •Higher mass and volume •More stray light

Selection of light filters:

Spectral bands of the camera are provided by the usage of light filters, each one mounted under its own CCD. It was generated taking into account the fact that in the gap between the last lens surface and CCD plane the camera shielding glass (K108 glass) and the CCD shielding glass (K8 glass) were installed. The light filter is sprayed on the mat made of radiation-resistant glass – grade K-108. The main optical filter characteristics are listed in table 6 and on the figure (12).

Table 6. Main optical filter characteristics [6]

λК…λД nm	Tmed %	Δτmed %	Δλ0,5 nm	Δλ0,1 nm	λКФ nm	λ,ДФ nm	τФ med %	τФ max %
520…780	≥ 60	≤ 5	510…790	500…800	300	1100	≤ 0,1	≤ 0,5

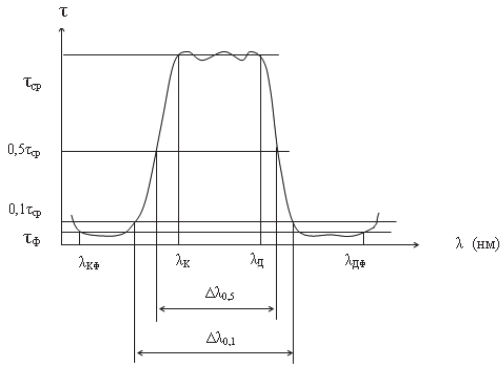

Fig. 12. Optical filter characteristics

In table 7 the advantages and disadvantage of different filter are shown.

Table 7. Filter types advantages and disadvantages [5]

Advantages	Disadvantages
GLASS FILTERS	
low impact of inclined entrance ray	limited filter assortments
robustness and long-term stability	very limited band-pass characteristics feasible
high transmission within a large bandwidth	fine tuning not possible
INTERFERENCE FILTERS	
any narrow bandwidth feasible	near parallel incidence of light required
spectral fine tuning feasible	sensitive against environmental impacts
steep edges in the spectral characteristics feasible	additional glass blocking filters necessary

Modulation Transfer Function (MTF)

Some major features are considered which influence the image quality from the spatial resolution point of view. A very effective way to describe the image quality is to use the Modulation Transfer Function MTF. Using the MTF approach, you can multiply all the image quality influencing MTF components of a linear system (or quasi linear system) which may base on different physical effects (e. g. optics, CCD,…) in order to create the system MTF [5].

Considering MTF dependencies the total MTF for the electro-optic camera can be estimated.

In general there are 3 factors determining MTF of the multiple-unit receiver on CCD basis:

- geometry MTF determined by the photosensitive element size and pitch between them;
- diffuse MTF given by spectral dependency of the silicon absorption and further charge diffusion spread;
- MTF determined by inefficiency of charge transfer in the register.

MTF geometrical multiplier is as follows:

$$MTF_g(\nu) = \frac{\sin(\pi.\nu.d)}{\pi.\nu.d} \tag{22}$$

where d is the pitch between elements and ν is spatial frequency.

If the apertures of the photodiode linear neighboring elements overlap and the overlap is equal to a, the geometry MTF becomes worse a little bit:

$$MTF_g(\nu) = \frac{\sin(\pi.\nu.d)}{\pi.\nu.d}.\frac{\sin(\pi.\nu.a)}{\pi.\nu.a} \tag{23}$$

Figure (13) shows dependences of the receiver geometrical MTF with pitch between elements d=7μm without apertures overlap and a=3 μm with aperture overlap.

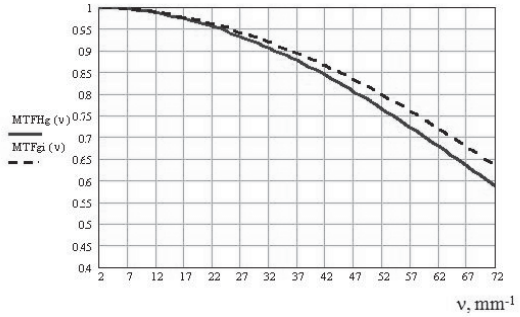

Fig. 13. Geometrical MTF of the CCD

Diffusion constituent of the MTF can be estimated theoretically if we have typical for RETICON technologies diffusion length and Spatial Charge Area (SCA):

$$MTF_{diffusion}(k,\nu) = \frac{1-\dfrac{\exp(-\alpha_k.dr)}{1+\alpha_k.L(\nu)}}{1-\dfrac{\exp(-\alpha_k.dr)}{1+\alpha_k.L_{diff}}} \tag{24}$$

where

$$L(\nu) = \frac{1}{\sqrt{\dfrac{1}{L_{diff}^{\ 2}} + (2\pi\nu)^2}} \tag{25}$$

where L_{diff} is the diffusion length, dr is the spatial charge area depth and α_k is the silicon absorption factor.

Following volumes of SCA and diffusion length were accepted for further calculations

$$dr = 5.10^{-4} \quad cm$$
$$L_{diff} = 50.10^{-4} \quad cm \tag{26}$$

Figure (14) shows diffusion MTF dependencies for monochromatic radiation from 500 to 900 nm.
MTF of inefficient charge transfer depends on the inefficiency volume and number of transfers.

$$MTF_{\varepsilon}(N,\nu) = \exp[-(1-\cos(\pi.\nu.2.d)).\varepsilon.N] \tag{27}$$

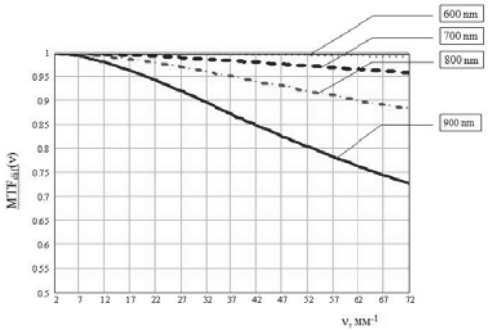

Fig. 14. Diffusion MTF of the CCD

where ε is the transfer inefficiency and N is the number of transfers in the CCD register.

Considering catalogue data (N=4000 for biphasic register when two registers are reading, $\varepsilon \le 5 \cdot 10^{-5}$) we have the inefficiency MTF given in figure (15).

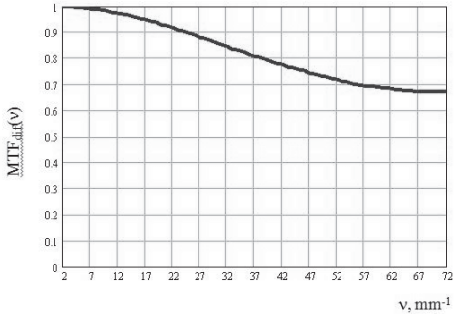

Fig. 15. Transfer inefficiency MTF for CCD

The additional factor effecting MTF during the survey is image "blur" within the time of signal storage in photodiodes. "Blur" appears only along the image movement that is perpendicular to the CCD line.

MTF_{mov}-MTF part conserned with image movement in focal plane during the signal storage time T_H with speed V_{fp}:

$$MTF_{mov} = \frac{\sin(\pi \cdot \nu \cdot V_{fp} \cdot T_H)}{\pi \cdot \nu \cdot V_{fp} \cdot T_H} \qquad (28)$$

The following figure (16) gives blur MTF for three storage times: T_0, $T_0/2$ and $T_0/4$.

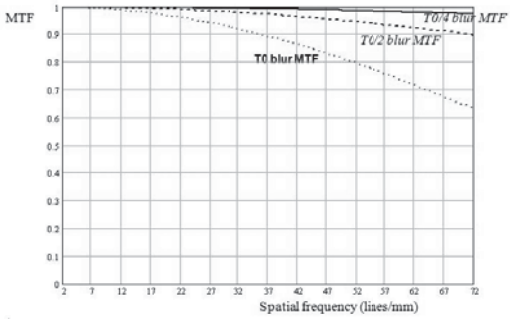

Fig. 16. MTFv dependence on the spatial frequency for different wavelengths of the incident radiation (with a maximal storage time d/ Vfp).

Total camera MTF in horizontal direction may be presented as follows (figure 17):

$$MTF_H(\nu) = MTF_{optics}(\nu) \cdot MTF_g(\nu) \cdot MTF_{diffusion}(\nu).MTF_\varepsilon(\nu) \qquad (29)$$

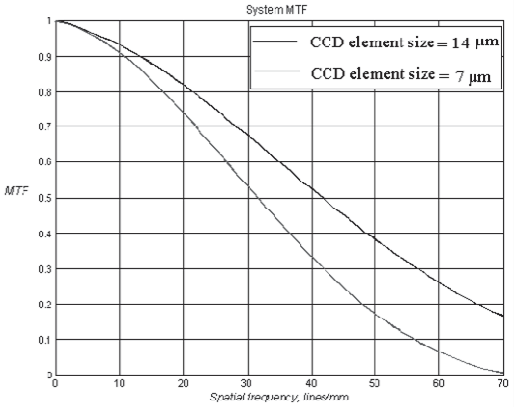

Fig. 17. Camera MTF at the deferent spatial frequency

where MTF_H is the total camera MTF in horizontal direction, MTF_{optics} is the optical system MTF, MTF_g is the MTF of the geometry, $MTF_{diffusion}$ is the diffusion MTF, and MTF_ε is the MTF of inefficient charge transfer.

$$MTF_{optics}(\nu) = \frac{2}{\pi}\left|\cos^{-1}\left(\frac{\nu}{\nu_\circ}\right) - \frac{\nu}{\nu_\circ}\sqrt{1-\left(\frac{\nu}{\nu_\circ}\right)^2}\right| \qquad (30)$$

Total camera MTF in vertical direction may be presented as follows (figure 17):

$$MTF_V(\nu) = MTF_{optics}(\nu) \cdot MTF_g(\nu) \cdot MTF_{mov}(\nu) \qquad (31)$$

where MTF_{mov} is MTF conserned with the image blur within the storage process.

Determine ACS Requirements

There are many activities going on to develop and test instruments, actuators, and algorithms to control the pointing with high accuracy. The obtained accuracies are between arcseconds and fractions of degrees. For mapping of the Earth's surface, deviations from the necessary precisions can be corrected using precise ground control points. The pointing stability is of more importance in order to maintain the ground sample distance and the image quality [8]. The MTF_{PS} of the platform has three major components

$$MTF_{PS} = MTF_{LM} \,.MTF_J \,.MTF_{\sin} \qquad (32)$$

where PS is platform stability, J is jitter, and sin is sinusoidal vibration)

The MTF degradation due to linear motion of the satellite is

$$MTF_{LM}(f_x) = \sin c(a_{LM}.f_x) \qquad (33)$$

where f_x is the spatial frequency, and a_{LM} the distance the target edge moves across the detector

pixel. MTF_{LM} only affects the MTF in the direction of the motion. The distance a_{LM} is $v \cdot \Delta t$. In many cases Δt is close to the dwell time and MTF_{LM} is approximately MTF_g. Figure (18) shows the influence of a_{LM} on the MTF_{LM}. MTF_{LM} with $a_{LM} = 1$ equals the detector MTF_g. The abscissa shows the spatial frequency normalized to the system dependend maximum value,

$$f = \frac{f_x}{f_{x,\max}} \tag{34}$$

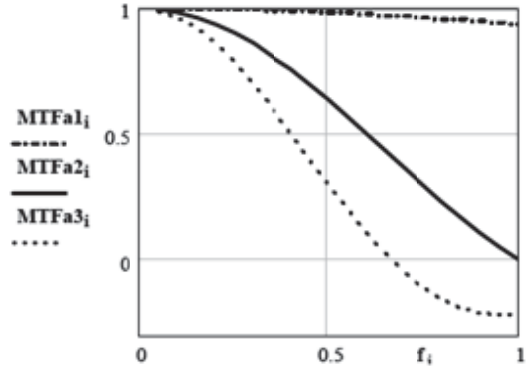

Fig. 18. Influence of a_{LM} on MTF_{LM} with a_{LM} = 0.1, 1, 1.5.GSD

For instance, with a detector pitch of 6.5 μm the spatial frequency of 150 cyc/mm equals $f_i = 1$. As a rule-of-the-thumb, when the linear motion causes an image shift less than about 20 % of the detector size, the effect on system performance is minimal.

For MTF_J (jitter or random motion) is assumed that the jitter is a superposition of different high-frequency motions so that the central limit theorem can be applied. It says that many random movements can be described by a Gaussian distribution

$$MTF_J(f_J) = \exp(-2\pi^2\sigma_J^2 f_J^2) \tag{35}$$

with σ_J the rms random displacement. Figure (19) shows the influence of σ on the MTF_J for σ = 0.1.x and σ = 1.x (x – detector element size).

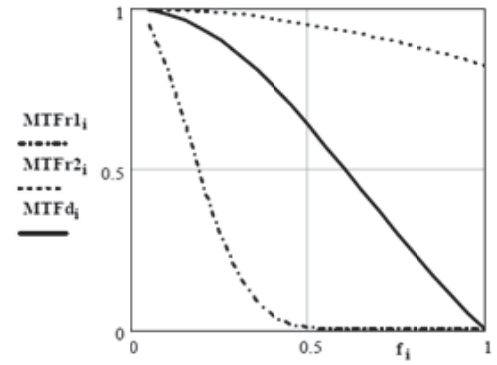

Fig. 19. Influence of s on the MTFJ with s = 0.1, 1.x. For comparison, MTF_D is also shown (MTF_d).

As a rule-of-the-thumb, when σ_J is less than about 10% of the detector size x, system performance is only minimal effected. Attitude control systems for pointing accuracies and stabilization to support high resolution functions on micro satellites are under development. In some cases, disturbing vibrations may also be avoided by simply switching off the active control functions during the relatively short imaging phase.

A sinoidal platform vibration is to be considered for systems with larger integration times (lower ground resolution) using

$$MTF_{\sin}(f_x) = J_0(2\pi a_{\sin} f_x) \tag{36}$$

$$t_{\text{int}} \succ\succ \frac{2\pi}{\varpi} \tag{37}$$

(J_0 – Bessel function of order zero, $a_{\sin}$ – amplitude of sinus wave)

Figure (20) shows the influence of the amplitude a of a sinusoidal platform vibration. As a rule-of-the-thumb, when the amplitude is less than 10 % of the pixel size, the effect on system performance is minimal.

Figure (21) shows the degradation of the detector MTF_g (with detector size x) due to the influence of

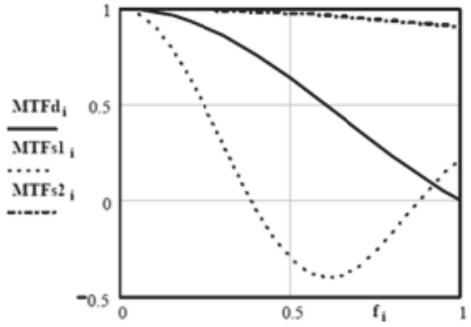

Fig. 20. Influence of the amplitude a of a sinusoidal vibration on $MTF_{\sin}$ with a = 0.1, 1 .x. For comparison, MTF_D is also shown (MTF_d)

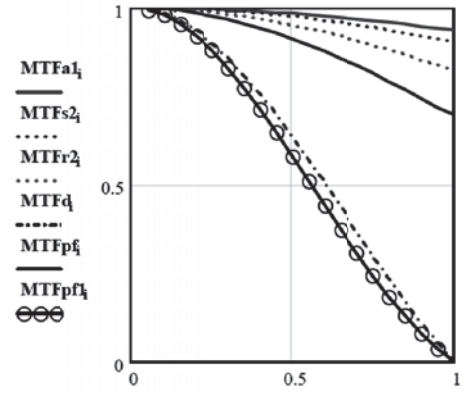

Fig. 21. Degradation of detector MTFD (MTF_d) due to MTF_{PS},(MTF_{pf}) consisting of MTF_{LM} (a = 0.2 .x), MTF_J (σ= 0.1 .x),$MTF_{\sin}$ (a = 0.1 .x). Resulting MTF is MTF_{pf1}

MTF_{PF} when for all three components of MTF_{PF} the rule-of-the-thumb parameters are applied (MTF_{LM} with a_{LM} = 0.2. x, MTF_J with σ = 0.1.x, MTF_{sin} with a = 0.1. x). The resulting MTF_{pfl} equals MTF_{SR} with neglected MTF_{optics} (MTF_{optics} = 1).

From an orbit altitude of 600 km, a GSD of 1 m equals an IFOV of 1.7 μrad or approximately 1/3 of an arcsec. During the dwell time, the drift shall be less than 20 % of the IFOV resulting in a drift rate of about 2.4 mrad/s or 8 arcmin/s in order to stay in the limit for minimal degradation of the MTF due to drift effects. When using the TDI principle to improve the SNR, for a 96 step TDI the tolerable drift rate becomes even 25 μrad/s or about 5 arcsec/s!

Required stability for imaging satellite is:

$$Stability = \beta \frac{R}{H} \times \frac{1}{T_{\text{int}}} \tag{38}$$

where R and H are resolution and orbit altitude respectively. Amount of β for the different resolution is shown in table (8).

The accuracy of pointing is:

$$\delta = \tan^{-1} \frac{0.1 \times S}{H} \tag{39}$$

where S is the swath width.

Table 8. β amount in the different resolution

Resolution (m)	β
>500	0.5
Between 500 and 100	0.33
Between 100 and 30	0.15
Between 30 and 5	0.1
<5	0.01

Data Volume & Transmission Rate

The data rate required for observation payloads depends on the resolution, coverage area, amplitude accuracy, and number of sensors. When the satellite is in low-Earth orbit, the satellite motion itself allows easy scanning of the Earth in the orbit plane. A separate mechanism in the sensor scans perpendicular to the orbit plane. The sensor generates an image composed of minimum resolvable elements called pixels. If the resolution element's diameter on the ground is d meters, directly below the satellite, the pixel size is d/h radians, where h is the satellite's altitude. The width of the sensor's scan angle, perpendicular to the satellite orbit, is θ_x also in radians [9].

The data rate, DR, generated by the sensor is:

$$DR = \frac{\theta_x V_N hsb}{d^2 q} \qquad bits/s \tag{40}$$

Where V_N: satellite's ground-track velocity, θ_x: width of the sensor's scan, perpendicular to satellite's orbit (radians), d: minimum diameter of pixel image projected on the ground, h: satellite's altitude, s: number of samples per pixel (typically 1 to 2), b: number of bits per sample (2^b amplitude levels), q: frame efficiency, fraction of time for data transmission (typically 0.90 to 0.95).

Mass, Volume, Power Consumption

Microelectronics

Since the launch of Landsat-1 in 1972, the progress in microelectronics has enabled more sophisticated instrument designs. The developments for the MESUR Network Mission may serve as an example, how much microelectronics technology may influence the overall mission design. The MESUR (Mars Environmental Survey) Network Mission concept consisted of up to 16 small spacecraft (that time planned to be launched in 2001). As often in extraterrestrial missions, there was a pressure to miniaturization by need. Reference mission was the MESUR Pathfinder Mission, one of the first missions under NASA's Discovery program of smaller, low-cost missions to be launched 1997.

In [3] the benefits have been assessed which may occur when the electronics technology used in the MESUR Pathfinder mission is replaced by advanced microelectronics technology. The MESUR Network study team found out that advanced microelectronics packaging technologies could be applied to the implementation of subsystem functions for

- The Attitude and Information Management System AIMS
- The Radio Frequency Subsystem RF
- The Power and Pyro Subsystem PP.

As a result, a factor of three or better reduction in mass, volume, and power consumption were projected relative to the MESUR Pathfinder baseline (see table 9).

Table 9. Projected total reduction in mass, volume, and power consumption for MESUR Network in comparison to MESUR Pathfinder [10]

	Pathfinder	Network	Next Reduction	Fractional
Mass	47 Kg	11 Kg	36 Kg	4.3x
Volume	46 dm^3	6.5 dm^3	39.5 dm^3	4.1x
Power	74 W	26 W	49 W	2.9x

The key to realize these reductions lies in the utilization of industry- based advanced microelectronics packaging technologies, including:

- Multichip module (MCM) technology
- Three-dimensional MCM stacking
- Die stacking for memory.

The leverage of these reductions to the spacecraft is obvious. The advanced microelectronics packaging technologies have been widely used for instance in a joint NASA/DLR study for the ROSETTA lander carrying among other cameras a stereo camera with 10 mm GSD

[5] and in a joint DLR/NASA three-line stereo camera concept for planetary exploration [6]. The effects have been remarkable. The latter concept resulted for instance in a very small stereo camera for a GSD of 20 m and a swath width of 250 km from an orbit altitude of 250 km, and with a weight of 2 kg and a power consumption of 12.5 Watts including a 1Gbit mass memory [10].

Detector

Pixel size influence - For mapping purposes the pixel size of the detector is projected via the focal length to the ground pixel size to be obtained, the smaller the detector elements x the shorter the focal length f (see figure 22). As an example, the stat-of-the-art CCD pixel size of 7µm results in a focal length of f = 4.2 m. Of course with smaller detector sizes less energy is integrated. If the sensitivity of the pixel element is not sufficient to obtain the necessary SNR, TDI needs to be applied or a so called slow-down mode allows enlarging the dwell time to the sufficient extent (should not be used in stereo imaging) [11].

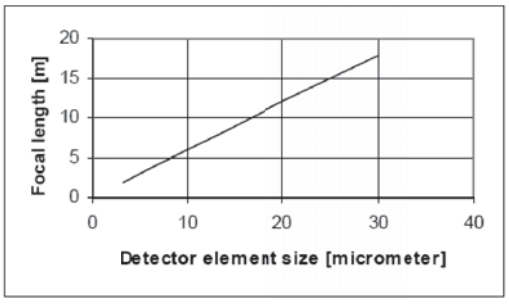

Fig. 22. Dependence between detector element size x and necessary focal length f for a given ground pixel size of X = 1 m from an orbit altitude of 600 km [8]

Impact of staggered configurations - Volumes and mass of optics depends significantly not only on the focal length and the aperture, but also on the image field size determined by the detector extensions. Using staggered line arrays, the following effects occur:

- Detector line length is halved
- Image field area is reduced to one quarter
- Focal length is halved
- the optics need to be of high quality for twice as many line pairs per millimeter with respect to the line pairs per millimeter necessary for the pixel size.

Staggered CCD-line arrays are used for instance in the SPOT-5 mission cameras HRS.

Optics

The focal length of high resolution space born sensors is determined by the physics laws and seems to be in contradiction to a small satellite concept in terms of mass and volume. The progress in production and test of optic systems enables now the utilization of highly efficient low-mass and low-volume optical telescopes for space applications. Examples are

- Use of aspheric lenses in refractive telescopes
- Use of folded arrangements for reflective telescopes (e. g. TMA)
- Use of sophisticated catadioptric telescopes.

Even if you can design a camera having weight compatible with a micro-satellite spacecraft, the volume of the lens system for high resolution space borne imagers is a problem if you think of the restricted size envelope for piggy-back launch opportunities.

The Technical University of Berlin recently performed a study concerning an interesting optics construction approach: the Dobson Space Telescope, DST, [2]. the core element of DST is a 20´´ f/5 Newton telescope. The secondary mirror will be placed via four 2.1 m booms when the spacecraft is already in orbit. In order to fulfill micro satellite requirements it is folded to minimal space during the launch. This type of telescopes called truss design Dobson was originally invented by ambitious amateur astronomers. To increase the resolution for remote sensing purposes, a “Barlow lens” with a factor of 2.5 pushes the focal ratio up to f/12.5 which assures maximum possible magnification and a ground pixel size of about 1m from a 700 km orbit.

Designing Result of Imaging Payload

The proposed system should provide the following main characteristics:

1. Resolution (GSD) of Earth surface survey from the altitude of 700 km: 50 m with swath width 50 km for operation of panchromatic camera;
2. Coverage area during Earth surface survey: 50 km x 2000 km
3. Earth surface remote sensing in spectral bands: 0.5 -0.9 µm for panchromatic camera;

The designing result of a panchromatic camera is listed in Table (10).

Table 10. The designing result of a panchromatic camera

Orbit altitude, km	700
Focal distance of objectives, mm	199.6
Lens aperture, D/F	1:5.4
Spectral bands, µm	0.5 – 0.9
Spatial resolution, (ground pixel projection) m	50
Swath, km	50
Number of equivalent CCD elements in each channel (14x14 µm)	1024
Equivalent CCD element size, µm	14x14
Integration Time, ms	7.2
Total MTF at the Nyquist frequency(35.6 line/mm), minimum	0.35
Signal to noise ratio, minimum	100
Video data quanting capacity, bit	8
Storage capacity, Gbit	2.0
Speed of data saving, Mbit/s	1.115
Data transfer rate to radio channel, Kbit/s	1330
Entrance pupil diameter, mm	37.0

Table 11. The designing result of a panchromatic camera, Continuance

Main wavelength, μm	0.5893
Angular field of view (2β), degrees	12
Distortion, %	< 0.1
Integral light transmission factor	>80%
Field of view illumination change, %	< 5
Pointing, degree	< 0.4
Stability, degree/second	< 0.08

Conclusion

This paper showed the problems connected with the imaging payload design. In this context the paper deals with such important parameters for imaging payload for remote sensing satellites like spatial resolution, MTF, signal, SNR, pointing accuracy and stability.

The systematical design and performance evaluation of the Imaging Payload for the remote sensing satellite technology has been described. It was done based on top-level customer system performance requirements and proposed approach for this purpose is based on SNR (detection) and MTF (resolution) analysis. The Imaging Payload was designed as a push broom scanner flying in a sun-synchronous polar orbit of 700 Km altitude and resolution of 50 meter.

References

[1] Jacobsen, K., High Resolution Satellite Imaging Systems – an Overview, PFG 6/2005, 487-496.

[2] Segert, T., Danziger, B. and Geithner, M., "The Dobson Space Telescope – A time shared Telescope for NEO and Earth Observation," Paper IAA-B4-0605 of the 4th International IAA Symposium on Small Satellites for Earth Observation, April 7-11, 2003, Berlin, German.

[3] Kramer, H. J., *Observation of the Earth and its Environment – Survey of Missions and Sensors*, 4th edition, Springer, Heidelberg, New York, 2002.

[4] Jahn, H. and Reulke, R., *Systemtheoretische Grundlagen optoelektronischer Sensoren*, Akademie Verlag, Berlin, 1995.

[5] Smith, W. J., *Modern Optical Engineering*, 2nd Edition, McGraw-Hill, 1996.

[6] *International Study on Cost-Effective Earth Observation Missions*, Edited Rainer Sandau, German Aerospace Center (DLR), Taylor & Francis the Netherlands, in print, 2006.

[7] Konecny, G., *Geoinformation: Remote Sensing, Photogrammetry and Geographic Information Systems*, Taylor & Francis, London and New York, 2003, 248 p.

[8] Holst, G. C., *CCD Arrays, Cameras, and Displays, SPIE Optical Engineering Press*, Bellingam, 1998.

[9] Wertz J. R. and Larson, W. J., *Space Mission Analysis and Design,* 3rd Edition, Microcosm Press, ElSegundo, California, 1999, 969 p.

[10] Alkalai, L. And Davidson, J. (Eds.), MESUR Network – Integrated Microelectronics Study. Final Report, JPL D-11192, January 7, 1994.

[11] Sandau, R., Hilbert, S., Venus, H., Fang, W.-C. and Alkalai, L., "A Three-Line Stereo Camera Concept for Planetary Exploration", *Paper IAA-L-0902 of the 2th International Conference on Low-Cost Planetary Missions*, April 16-19, 1996, Laurel, Maryland, USA.

[12] Holst, G. C., *Electro-Optical Imaging System Performance*, SPIE Optical Engineering Press, 1995.